Investigation of Transition Phenomenon from Rotating Cavitation to Attached Asymmetric Cavitation by Coupled Analysis of One-Dimensional Flow Path Model of 3-Blade Inducer and Shaft Vibration System

Tsuyoshi Inoue [1] , Hirohisa Ohama [2]
Nagoya university, Nagoya, Aichi, 464-8603, Japan

Yuki Imaeda [3]
Mitsubishi Heavy Industries, Ltd, Komaki, Aichi, 485-8561, Japan

Satoshi Kawasaki [4], Takashi Shimura [5], Mitsuru Shimagaki [6]
Japan Aerospace Exploration Agency(JAXA), Kakuda Space Center, Kakuda-shi, Miyagi 981-1525, Japan

Masaharu Uchiumi [7]
Muroran Intsitute of Technology, Muroran, Hokkaido, 050-8585, Japan

1 Professor, Department of Mechanical Systems Engineering.
2 Master student, Department of Mechanical Systems Engineering.
3 Engineer, Integrated Defense and Space Systems, Aircraft and Missile Systems Division.
4 Senior Researcher, Research and Development Directorate.
5 Technical Advisor, Research and Development Directorate.
6 Senior Researcher, Research and Development Directorate.
7 Professor, Aerospace Plane Research Center.

Abstract

During the development process of the turbopump for a rocket engine currently in operation in Japan, various problems of shaft vibration have been reported. Among them, vibration problems caused by dynamic fluid flow phenomena in the inducer, such as rotation cavitation (RC) and attached asymmetric cavitation (AAC), are known to be major factors that impair the stability of the system. Many theoretical analyses have been carried out to elucidate the causes of RC, particularly studies using computational fluid dynamics (CFD). AAC is a phenomenon in which the cavity swirls in synchronization with the velocity of the cascade causing an increase in the shaft vibration and a decrease in the inducer head coefficient. AAC in three bladed inducers was investigated experimentally and a transition from RC to AAC was observed. However, there has been no analytical investigation of this transition phenomenon from RC to AAC. In this study, the transition from RC to AAC was investigated using a one-dimensional flow-path model of the inducer. The occurrence of this transition was evaluated by comparison with the experimental results. Furthermore, a coupled analysis of the rotor and fluid systems was performed. These results were compared with the experimental results and discussed.

1. Introduction

The turbopumps in rocket engines must operate at high speed and low suction pressure to reduce its size and weight. During development of turbopump for the rocket engine, various problems of shaft vibration have been reported [1]. In particular, cavitation occurs at the inlet of the axial inducer, causing various vibration problems. de Bernardi [2] further reduced the inlet pressure after the onset of cavitation and showed how various cavitation patterns occur continuously on the performance curve of a liquid hydrogen inducer. Vibration problems caused by dynamic fluid flow phenomena [3] such as cavitation surge, rotation cavitation (RC), attached asymmetric cavitation (AAC), and rotating stall-like phenomenon. Kamijo et al. explained them as major factors that impair the stability of the system [4] [5].

RC is a phenomenon in which cavity volume fluctuations propagate through inducer blades one after another [5][6]. Shimura et al. [7] identified pump dynamic characteristic coefficients (cavitation compliance and mass flow gain factor) through turbopump tests using two types of inducer liners and reported the effect of liner shape on turning cavitation suppression.

Several theoretical analyses have been conducted to elucidate the causes of RC. Tsujimoto et al. [8] modeled the cavity volume fluctuation characteristics using the pump dynamic characteristic coefficient, performed linear analysis, and explained the occurrence of RC. He then clarified that RC

is a different phenomenon from rotating stall. Joussellin & de Bernardi et al [9] also developed a numerical model that can analyze cavitation instability in similar inducers, and Pilipenko et al [10] used this model to calculate the flow around the cavity and investigated the characteristics of the cavitation. Watanabe et al. [11] predicted RC by singular point analysis using a closed cavity model without using the pump dynamic characteristic coefficients and showed that the tendency of the propagation velocity ratio qualitatively agrees with the experimental results.

To understand and improve the prediction of cavitation instabilities, LEGI, Safran Aircraft Engines, and the French space agency CNES have collaborated to advance numerical and experimental analyses [12]. Reboud & Delannoy et al. [12] and Delannoy & Kueny et al. [13] simulated the cavitation behavior of an inducer using a two-dimensional numerical model of unsteady cavitation flow developed at LEGI. Coutier-Delgosha et al. [14] adapted this model to a two-dimensional blade cascade. Joussellin et al [15] investigated cavitation flow in a rocket engine turbopump inducer experimentally and numerically, and observed rotational cavitation phenomena in the numerical analysis under certain conditions, which were in good agreement with experimental observations. Coutier-Delgosha et al. [16] observed two different unstable forms of rotational cavitation (sub-synchronous and super-synchronous) in a four-blade turbopump inducer in a rocket engine using two-dimensional numerical model of unsteady cavitation, and discussed their onset mechanisms. They also presented limits of its stability with mass flow rate and cavitation number, and made qualitative comparisons with experiments [17]. Angelo Cervone et al. [18] observed cavitation surges, rotational stalls, and self-excited vibrations leading to severe surge mode instabilities in the three-blade inducer, on the other hand, reported that few vibration phenomena were detected in the MK1 inducer.

Several experimental studies were also investigated. Pace et al [19] performed experiments on a three-bladed inducer and compared the hydraulic performance and flow instability of the pump in non-cavitation and cavitation conditions with experimental data from other similar inducers. Wan et al. [20] defined and validated a reduced-order approach to infer key parameters such as cavitation compliance, K, and mass flow gain factor, M, from the unsteady pressure measurements using single sensor. Sales and Pasini [21] used the modular multi-actuator disk approach and expanded a cavitating inducer model developed in the 90 s for the assessment of azimuthal instabilities with a particular focus on rotating cavitation. Furthermore, Pasini et al [22] developed a dynamic model of unsteady flow in an blade cascade based on experimental data and a suitable description of mean flow and cavitation oscillations, which was used to estimate the intensity of the flow oscillations at the operating conditions of the inducer. Pace et al [23] detected, and identified flow instabilities occurring in inducers by spectral analysis of pressure measurements simultaneously made in both stationary and rotating frames by multiple transducers. Valentini et al. [24] showed the extensive experimental results and their characterization of the rotordynamic forces acting on a three-bladed, tapered-hub, variable-pitch inducer using the Cavitating Pump Rotordynamic Test Facility (CPRTF) at ALTA S.p.A.

With recent improvements in computing power, many studies on RC using computational fluid dynamics (CFD) analysis have been reported. Iga et al. [25] reproduced the cavitation instability phenomenon, including RC, by CFD analysis for three cascades and discussed the mechanism of its occurrence. Hosangadi et al [26] used CRUNCH CFD to simulate cavitation performance and rotational cavitation for a SSME low-pressure fuel pump (LPFP) sub-scale configuration under off-design flow conditions with backflow vortices on the leading edge. Benoît Pouffary et al [27] simulated the cavitation behavior of a rocket engine turbopump inducer using CFD code FINE/TURBO™, and observed occurrence of steady or unsteady behavior with sub-synchronous or super-synchronous regions. Fortes-Patella et al. [28] observed two different unstable forms of cavitation in a four-blade rocket engine turbopump inducer using a two-dimensional numerical model of unsteady cavitation, investigated their mechanisms, and estimated stress fluctuations induced in the blades. Further, Byungjin et al. [29] reported that the transition from RC to cavitation surge could be reproduced by CFD analysis while considering the change in flow rate in the piping system upstream of the inducer. Chang-Ho Choi et al [30] conducted experiments and simulations of cavitation flow around turbopump inducer using the CFD code FINE/TURBO to investigate qualitatively the relationship between the strength of the reverse flow at head breakdown, the occurrence of rotating cavitation, and shaft vibration.

Additionally, research using simple One-dimensional computer-aided engineering (1D-CAE) analysis method has also been conducted. Shimura et al. [31] and Kawasaki et al. [32] represented the three-blade inducer as a set of three one-dimensional flow path models using commercial software (Simcenter Amesim) and demonstrated that the RC phenomenon can be expressed and explained by this model.

Attached cavitation is a phenomenon in which the cavity swirls in synchronization with the velocity of the cascade, i.e., the cavity sticks to the blade in a rotating coordinate synchronous to the shaft rotation. When the attached cavity is not symmetric with respect to the rotation axis, which is the case of attached asymmetric cavitation (AAC), it causes an increase in shaft vibration and a decrease in the inducer head coefficient. This is a problem that needs to be addressed in the inducer design process and many studies have been conducted.

Horiguchi et al. performed a two-dimensional analysis on the alternate blade cavitation (ABC) of an even-numbered blade inducer, clarified the occurrence of bifurcation in the cavity length as the cavitation number decreased, and explained the experimental results [33]. Further, they investigated the case of three bladed inducers as well and reported that no bifurcation of the cavity length was observed [34]. Campos-Amezcua et al. [35] simulated unsteady cavitation flow of axial inducer using a 2D blade cascade model, and investigated local cavitation instabilities such as alternating blade cavitation and rotating cavitation.

Lettieri et al. [42] used a four bladed inducer as representative of a low-pressure liquid oxygen pump (LPOP) inducer of modern design, investigated its dynamic behavior such as rotating cavitation (RC) and ABC, and discussed the physical mechanism of onset of RC. They also investigated and obtained experimental results useful for diagnostics of inducer dynamic behavior during rotating cavitation (RC), alternate blade cavitation (ABC), and cavitation surge (CS) [43]. Vermes et al. [44] presented a source term based model of rotating cavitation (RC) for stability assessment in rocket engine turbopumps, and showed significant reduction of its computational cost keeping its significant accuracy.

Kobayashi [36] experimentally investigated AAC in three bladed inducers and clarified that its occurrence became remarkable when imbalance increased. Yoshida et al. [37] reported an experimental result on the transition from RC to AAC when the cavitation number decreased, and further asserted that both the average cavitation length and difference in cavitation length between flow paths also increased before occurrence of this transition. Furthermore, a decrease in the head coefficient and bifurcation of the cavity length were observed when the transition from RC to AAC occurred. However, to the best of authors' knowledge, these are only experimental results and there has been no analytical investigation of this transition phenomenon from RC to AAC. Hadavandi et al. [38] reported the experimental characteristics of flow instability due to cavitation in a high-head three-bladed inducer, in particular, the transition phenomenon from RC to AAC observed in the experiment. However, there has been no analytical investigation of this transition phenomenon from RC to AAC.

In this study, the transition from RC to AAC was investigated using the one-dimensional flow path model of the inducer constructed by Shimura et al., while taking various parameter conditions into consideration [31][32]. Additionally, an inducer test was carried out in a water tunnel and the transition from RC to AAC were observed. The results of this experiment were considered together in conjunction with the experimental results reported in the literature [36][37].

The occurrence of transition from RC to AAC obtained in the analysis using the one-dimensional flow path model of the fluid system was evaluated by comparison with the experimental results [31]. Furthermore, a coupled analysis of the rotor and fluid systems was performed considering the shaft imbalance and the effect of the AAC on the shaft vibration was investigated. The results were compared with the experimental results and discussed.

Nomenclature

Variables	Description	Unit
Q_{1a}, Q_{1b}, Q_{1c}	Volume flow rate at first half of flow path in inducer	m^3/s
Q_{ma}, Q_{mb}, Q_{mc}	Volume flow rate at middle part of flow path in inducer	m^3/s
Q_{2a}, Q_{2b}, Q_{2c}	Volume flow rate at last half part of flow path in inducer	m^3/s

$Q_{ab},\ Q_{bc},\ Q_{ca}$	Volume flow rates of leakage flow from flow path A to flow path B, flow path B to flow path C, and flow path C to flow path A	m^3/s
P_{1a}, P_{1b}, P_{1c}	Pressure at first half of flow path in inducer	Pa
P_{ma}, P_{mb}, P_{mc}	Pressure at middle part of flow path in inducer	Pa
P_{2a}, P_{2b}, P_{2c}	Pressure at second half of flow path in inducer	Pa
P_{in}, P_{out}	Pressure at inlet and outlet of inducer	Pa
Q_{in}, Q_{catch}	Volume flow rate at inlet and outlet of inducer	m^3/s
R_{1a}, R_{1b}, R_{1c}	Pipe resistances at first half of flow path in inducer	$kg \cdot m^{-7}$
R_{2a}, R_{2b}, R_{2c}	Pipe resistances at second half of flow path in inducer	$kg \cdot m^{-7}$
R_{in}, R_{catch}	Pipe resistances of upstream and downstream of inducer	$kg \cdot m^{-7}$
R_{ab}, R_{bc}, R_{ca}	Pipe resistances of leakage flow path	$kg \cdot m^{-7}$
C_f	Flow coefficient	NA
α_{pr}	Head distribution ratio	NA
Q_d	Design flow rate of liquid hydrogen turbo pump	m^3/s
n_b	Number of flow paths	NA
U_t	Tip speed of inducer	m/s
L_h	Chord length	m
γ_{ind}	Blade angle	rad
σ	Cavitation number $(P_{in} - P_v)/(\rho {U_t}^2/2)$	NA
Cb	Cavitation compliance	NA
Mb	Mass flow gain factor	NA
ρ	Density of liquid hydrogen	kg/m^3
ν	Kinematic viscosity of liquid hydrogen	Pa s
P_v	Saturated vapor pressure of liquid hydrogen	PaA
ω	Rotational speed of turbopump	rpm
C_r	Steady tip clearance	m
ε	Whirl amplitude ratio(r/C_r)	NA
m_1	Rotor mass	kg

k, c	Support stiffness and damping coefficients of rotor system	N/m, Ns/m
U	Rotor unbalance	Kgm
x, y	Rotor position	m
F_{ind_x}, F_{ind_y}	Fluid force caused at inducer	N
$\bar{\beta}_{nom}$	Average value of the relative flow angle at flow path inlet	rad
l_{nom}, l_a, l_b, l_c	Nominal cavity length, and cavity length in flow path A, B, and C	m
w_{nom}, w_a, w_b, w_c	Nominal cavity width, and cavity width in flow path A, B, and C	m
h	Cavity height	m
V_{nom}	Nominal cavity volume	m^3
C_p	Pressure coefficient	NA

2. Experiment of transition from RC to AAC

First, the occurrence of transition from RC to AAC was confirmed in the experiment that was conducted using the test facility at the JAXA Kakuda Space Center.

2.1. Experimental Facility

The test facility of water tunnel and inducer are shown in Fig. 1 and Fig. 2. To enable visualization of cavitation, a straight acrylic casing was used as the casing for the inducer. An ultrasonic flowmeter and turbine flowmeter were used for flow measurements and the flow-rate ratio Q/Q_d was controlled using valves. The inducer was driven by using 185 kW DC motor, and its rotation speed was maintained at constant. The test loop pressure can be pressurized and depressurized by a pressure regulating piston installed upstream of the inducer. The water temperature in the test loop can be kept constant to some extent by a heat exchanger. Other detail parameters and information are shown in the previous paper [39].

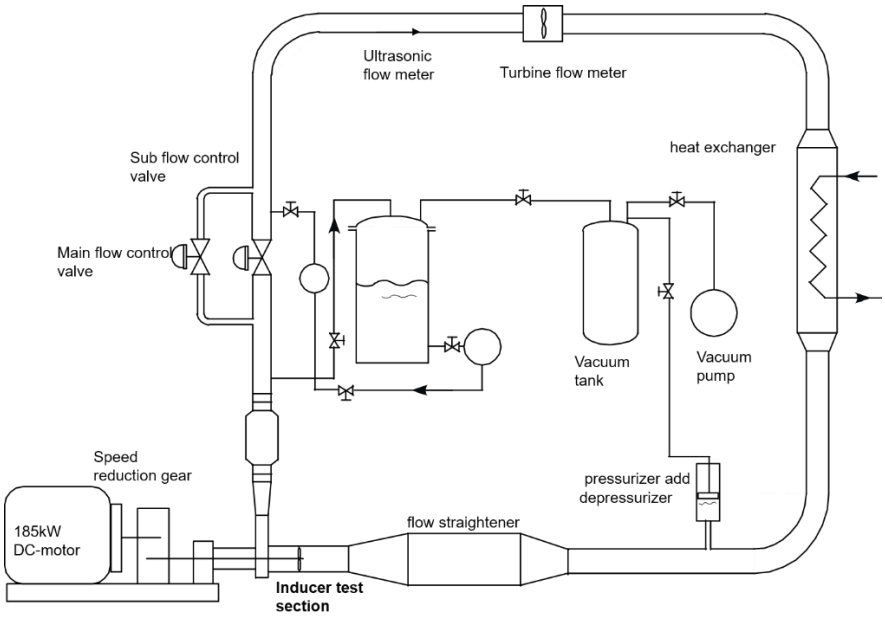

Fig. 1 The test facility

Fig. 2 Test inducer

2.2. Cavitation and its effect on shaft vibration

In this section, the outline of the experiments is presented. During the experiment, the inlet pressure of the inducer was gradually reduced to reduce the cavitation number. The rotational speed was constant at 6000 rpm (100 Hz) and the cavitation number was reduced from 0.25 to 0.015, as shown in Fig. 3. Subsequently, the influence of cavitation on the shaft vibration, occurrence of RC, and its transition to AAC were observed.

It should be noted that the speed of the actual rocket turbopump is 42,500 rpm, while the experiments using water as the working fluid was conducted at 6000 rpm due to equipment limitations. This is because it is known [40] that the cavitation performance of inducers can be compared and evaluated by using parameters such as cavitation number σ to eliminate the effect of rotation speed.

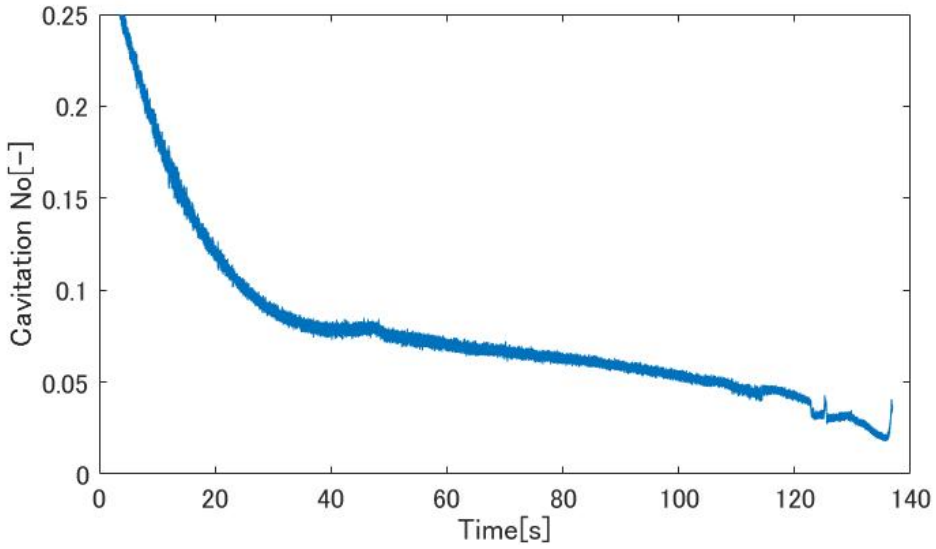

Fig. 3 Time history of cavitation number

Table 1 shows the cavitation number when RC occurs, the occurrence of the transition to AAC, and the cavitation number at this transition. Symbol ○ denotes occurrence and symbol × denotes non-occurrence. RC occurred when the cavitation number was in the range of approximately 0.06 to 0.07. Subsequently, a transition from RC to AAC was observed when the cavitation number was in the range of approximately 0.02 to 0.04.

Table 1 Test results

Ratio of flow rate Q/Q_d	Cavitation number σ when RC occurs	Occurrence of transition from RC to AAC ○: Occur ×:Not occur	Cavitation number σ when the transition to AAC occurs
1.10	0.07	○	0.024
1.05	0.06	○	0.038

2.2.1. Measurement of shaft vibration

Fig. 4 (case of flow-rate ratio Q/Q_d = 1.05 in Table 1) shows the changes in the magnitude and frequency of the shaft vibrations using the experimental data in which the transition from RC to AAC was observed. The experiment was performed by reducing the cavitation number gradually. A frequency component appeared at a frequency of approximately 1.2 times the rotational speed when

the cavitation number was in the range of approximately 0.06 to 0.07.

This is an asynchronous vibration caused by the fluid force consequent to occurrence of RC. When the cavitation number was reduced further in the range of 0.02 to 0.04, the asynchronous component became entrained in the synchronous component. The high-speed camera record shows the occurrence of AAC on the blade. This causes a fluid imbalance and the synchronous vibration component increases sharply and significantly, which is a transition phenomenon from RC to AAC. In the experiment, the shaft vibration amplitude at the occurrence of AAC was approximately 1.5 times the vibration at the occurrence of RC.

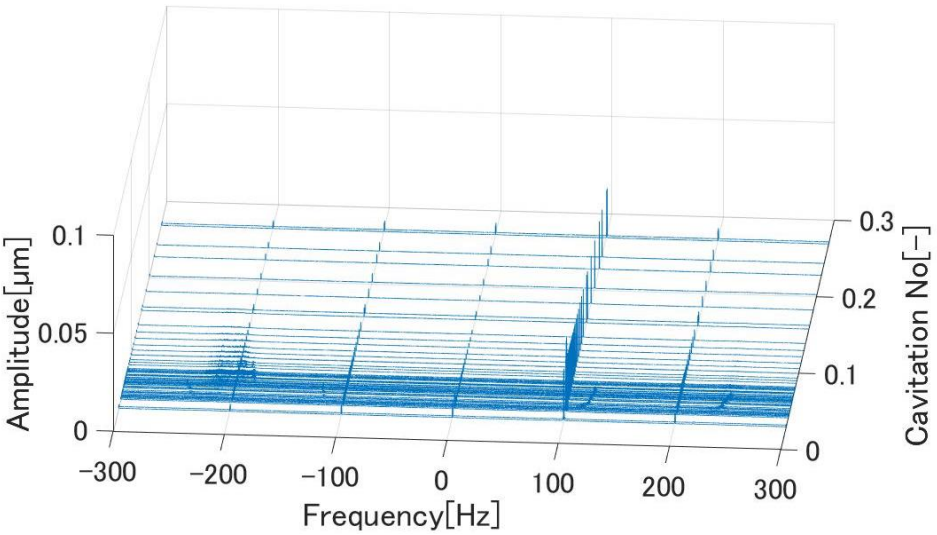

Fig. 4 (Case 04) Frequency change of shaft vibration in the experiment

3. One dimensional modeling of inducer flow paths

3.1. One dimensional modeling of flow

This study analytically investigates a three-bladed inducer (Fig. 2) in which an axial flow impeller pressurizes the propellant upstream of the turbopump. First, the one-dimensional flow path model of the inducer used in this study was explained [31][7]. Fig. **5** shows the fluid flow through the one-dimensional flow path model of the three-bladed inducer [31]. The model is represented in a rotational coordinate system that rotates synchronously with shaft rotation with the following two assumptions: cavitation occurred in each flow path and its effect appeared in the middle part of the flow path. The

leak flow generated in the inducer tip is expressed as a pipe with an orifice connected from the middle part of the flow path to the inlet of the adjacent flow path.

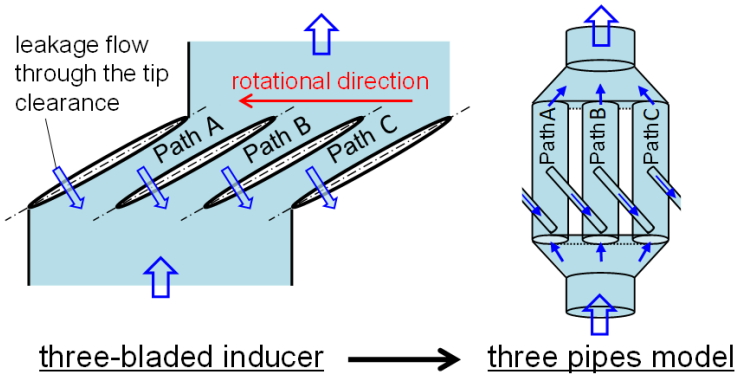

(a) One dimensional modeling of inducer with main three pipes and leakage flow pipes

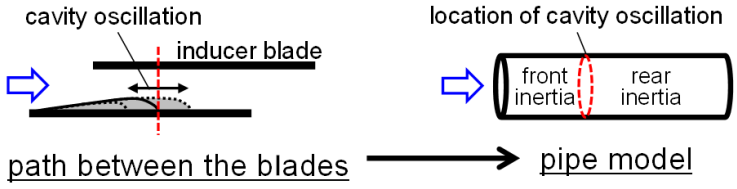

(b) One dimensional modeling in the pipe

Fig. 5 One dimensional flow path model of inducer

3.2. One dimensional modeling of inducer

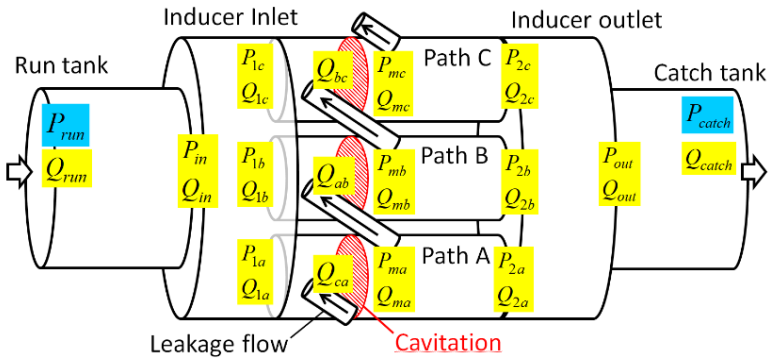

Fig. 6 One dimensional flow path model of three bladed inducer

Fig. 6 shows a one-dimensional flow path model of the inducer flow. The independent variables are pressure P_{in} and flow rate Q_{in} at the inducer inlet; pressure P_{out} and flow rate Q_{out} at the inducer outlet; inlet pressure $P_{1i}(i = 1,2,3)$ and flow rate $Q_{1i}(i = 1,2,3)$ in each flow path; middle part pressure $P_{mi}(i = 1,2,3)$ and flow rate $Q_{mi}(i = 1,2,3)$ in each flow path; outlet pressure $P_{2i}(i = 1,2,3)$ and flow rate $Q_{2i}(i = 1,2,3)$ in each flow path; and flow rate Q_{ab}, Q_{bc}, Q_{ca} in the leakage flow paths. The supply pressure P_{run} upstream and discharge pressure P_{catch} downstream of the turbo pump are given as boundary conditions. The working fluid is considered incompressible. The inducer model flow shown in Fig. 6 has been formulated using a set of nine fundamental equations. The equations shown in this section are dimensional unless otherwise stated.

3.2.1. Equation of motion in the first half of the flow path

The equation of motion for the first half of the flow path is expressed as follows:

$$\begin{aligned} &P_{1*} - P_{in} + \rho L_{1*}\frac{dQ_{1*}}{dt} + R_{1*}{Q_{1*}}^2 = 0 \\ &L_{1*} = \frac{l_{1*}}{A_{1*}}, \quad R_{1*} = \frac{\rho l_{1*}}{2{A_{1*}}^2 D_{1*}}\lambda_{1*} \qquad (*=a,b,c) \end{aligned} \tag{1}$$

The $L_{1*}(*= a, b, c)$ in the third term on the left side indicates the inertance of each channel, and the $R_{1*}(*= a, b, c)$ in the fourth term indicates the resistance of each channel. Because the approximate value of the Reynolds number of the analytical model is 2.92×10^7 and large, Nikuradse's equation [32] for the high Reynolds number region is used for the pipe friction coefficient.

$$\lambda = 0.0032 + 0.221\mathrm{Re}^{-0.237} \tag{2}$$

3.2.2. Equation of motion in the latter half of the flow path

The equation of motion for the latter half of the flow path is expressed as follows:

$$\begin{aligned} &P_{2*} - P_{m*} + \rho L_{2*}\frac{dQ_{2*}}{dt} + R_{2*}{Q_{2*}}^2 = 0 \\ &L_{2*} = \frac{l_{2*}}{A_{2*}}, \quad R_{2*} = \frac{\rho l_{2*}}{2{A_{2*}}^2 D_{2*}}\lambda_{2*} \qquad (*=a,b,c) \end{aligned} \tag{3}$$

As in Section 3.2.1, $L_{2*}(*= a, b, c)$ in the third term on the left side indicates the inertia of the flow path, and $R_{2*}(*= a, b, c)$ in the fourth term indicates resistance.

3.2.3. Dynamics of the fluid at the upstream pipe

The dynamics of the fluid upstream of the inducer from the run tank to the inlet of the inducer are formulated as follows:

$$\begin{aligned} &\rho L_{in}\frac{dQ_{in}}{dt}+P_{in}-P_{run}+R_{in}{Q_{in}}^{2}=0 \\ &L_{in}=\frac{l_{in}}{A_{in}},\quad R_{in}=\frac{\rho l_{in}}{2{A_{in}}^{2}D_{in}}\lambda_{in}+\frac{\rho}{2{C_f}^{2}{A_{in\_orf}}^{2}}+\frac{\rho}{2{A_{in}}^{2}} \end{aligned} \tag{4}$$

R_{in} is the resistance of the flow path. The losses at the bending and connecting parts of the channels have not been considered.

3.2.4. Dynamics of the fluid at the downstream pipe

As described in Section 3.2.3, the dynamics of the fluid flow downstream of the inducer from the outlet of the inducer to the downstream catch tank is formulated as follows:

$$\begin{aligned} &\rho L_{catch}\frac{dQ_{catch}}{dt}+P_{catch}-P_{out}+R_{catch}{Q_{catch}}^{2}=0 \\ &L_{catch}=\frac{l_{catch}}{A_{catch}},\quad R_{catch}=\frac{\rho l_{catch}}{2{A_{catch}}^{2}D_{catch}}\lambda_{catch}+\frac{\rho}{2{C_f}^{2}{A_{catch\_orf}}^{2}}+\frac{\rho}{2{A_{catch}}^{2}} \end{aligned} \tag{5}$$

3.2.5. Flow rate dynamics due to cavity volume fluctuation

In this study, based on the observation of experimental results, cavitation was modeled as occurring only in the first half of the cascade [31]. The effect of cavity volume fluctuation is expressed in the middle part of the flow path as follows:

$$Q_{m*}-Q_{1*}+Cb_{nom}\frac{dP_{1*}}{dt}+Mb_{nom}\frac{dQ_{1*}}{dt}=0\quad (*=a,b,c) \tag{6}$$

Here, the pump dynamic characteristic coefficients (cavitation compliance Cb and mass flow gain factor Mb) have been used to represent the flow rate fluctuation due to the cavity volume change. Cavitation compliance Cb represents the rate of change in cavity volume with respect to changes in inlet pressure in the flow path, and mass flow gain factor Mb represents the rate of change in cavity volume with respect to changes in inlet flow rate in the flow path.

The subscript “nom” in the equation indicates a nominal value determined for all three flow paths. In this analysis model, the nominal values of the cavitation compliance Cb and mass flow gain factor Mb were determined by dimensionalizing the dimensionless values of Mb^* and Cb^*; they were obtained through dynamic characteristic test of a turbopump for a rocket engine with a thrust of 100 tons [7] in a situation where RC occurs. The following formulas were used:

$$
\begin{aligned}
Cb^* &= 6.881\exp(-59.11\sigma) \\
Cb_{nom} &= 3Cb^* \frac{2\pi D_{ind} A_{ind}}{{n_b}^2 \rho {U_t}^2} \\
Mb^* &= 3.491\exp(-25.5\sigma) \\
Mb_{nom} &= Mb^* \frac{\pi D_{ind}}{n_b {U_t}^2}
\end{aligned}
\tag{7}
$$

Here, $n_b = 3$. The cavitation number σ of all three flow paths is represented by the steady-state value of the inlet pressure of flow path A, $\bar{P}_{1a}$, using the following equation:

$$
\sigma = \frac{2\left(\bar{P}_{1a} - P_v\right)}{\rho {U_t}^2} \tag{8}
$$

Kamijo [8] explained that RC occurs when the following condition using cavitation compliance Cb and mass flow gain factor Mb is satisfied:

$$
\frac{Mb}{Cb} > 2\left(1+\sigma\right)\cot\bar{\beta}_1 \tag{9}
$$

From the above background, the cavitation compliance Cb, mass flow gain factor Mb, and cavitation number σ are considered important quantities for the transition phenomenon from RC to AAC.

3.2.6. Pressure rise equation in the first half of the flow path

For the pressure rise by the inducer, the following simple model including the test results of the inducer is used for the first half of the flow path :

$$
\begin{aligned}
&P_{m*} - P_{1*} + \mu_f Q_{1*} - P_f = 0 \\
&\mu_f = \frac{0.15\rho {U_t}^2 \alpha_{pr}}{Q_d}, \quad P_f = 0.3585\alpha_{pr}\rho {U_t}^2 \qquad (* = a, b, c)
\end{aligned}
\tag{10}
$$

Here, α_{pr} is the head distribution ratio, which refers to the head ratio of the first half of the flow path to the total pump head.

3.2.7. Pressure rise equation in the latter half of the flow path

Similar to Section 3.2.6, the following simple model was used for the pressure rise in the latter half of the flow path:

$$
\begin{aligned}
&P_{out} - P_{2*} + \mu_r Q_{2*} - P_r = 0 \\
&\mu_r = \frac{0.15\left(1-\alpha_{pr}\right)\rho {U_t}^2}{Q_d}, \quad P_r = 0.3585\left(1-\alpha_{pr}\right)\rho {U_t}^2 \qquad (* = a, b, c)
\end{aligned}
\tag{11}
$$

3.2.8. Leakage flow rate

The leakage flow to the adjacent flow path through the clearance between the inducer blade tip and casing is formulated as follows :

$$
\begin{aligned}
&P_{in} - P_{ma} + \rho L_{ab} \frac{dQ_{ab}}{dt} + R_{ab} Q_{ab}{}^2 = 0 \\
&P_{in} - P_{mb} + \rho L_{ab} \frac{dQ_{ab}}{dt} + R_{bc} Q_{bc}{}^2 = 0 \\
&P_{in} - P_{mc} + \rho L_{ab} \frac{dQ_{ab}}{dt} + R_{ca} Q_{ca}{}^2 = 0 \\
&L = \frac{l_{leak}}{A_{leak}}, \quad R_{ab} = \frac{\rho}{2 C_f{}^2 A_{ab}{}^2}, \quad R_{bc} = \frac{\rho}{2 C_f{}^2 A_{bc}{}^2}, \quad R_{ca} = \frac{\rho}{2 C_f{}^2 A_{ca}{}^2}
\end{aligned}
\tag{12}
$$

Here, $A_{**}(** = ab, bc, ca)$ is the leakage area at each blade tip determined using the rotor displacement (x, y).

3.2.9. Flow rate at branch point and confluence point

Considering the leakage flow rate, the following relationship holds between the flow rates at the branch point upstream of the inducer and the confluence point downstream of the inducer:

$$
\begin{aligned}
&Q_{in} = Q_{1a} + Q_{1b} + Q_{1c} - Q_{ab} - Q_{bc} - Q_{ca} \\
&Q_{catch} = Q_{2a} + Q_{2b} + Q_{2c}
\end{aligned}
\tag{13}
$$

Similarly, the branches of the leak flow in the middle parts of the flow paths are expressed as follows :

$$
\begin{aligned}
&Q_{ma} = Q_{2a} + Q_{ab} \\
&Q_{mb} = Q_{2b} + Q_{bc} \\
&Q_{mc} = Q_{2c} + Q_{ca}
\end{aligned}
\tag{14}
$$

The set of the nine equations above is the governing equation for the one-dimensional flow model of the inducer flow.

3.3. Modeling of pump rotor system

A rigid rotor model as shown in Fig. 7 is considered.

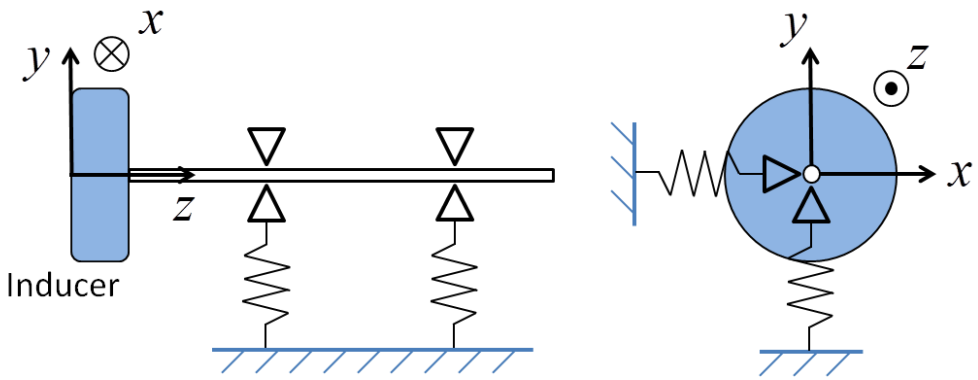

Fig. 7 Rigid rotor model of turbopump

The left side of the inducer is the upstream (suction side) and the right side is the downstream (discharge side). The origin of the reference flame was taken at the left end of the inducer and the z axis was taken in the axial direction. The equation of motion of the rotor system in the dimensional form is as follows :

$$\begin{aligned} m_1\ddot{x} &= -c\dot{x} - kx + \left\{F_{ind\_x}(x,y) + F_{cnt\_x}\right\} + U\omega^2\cos\omega t \\ m_1\ddot{y} &= -c\dot{y} - ky + \left\{F_{ind\_y}(x,y) + F_{cnt\_y}\right\} + U\omega^2\sin\omega t \end{aligned} \tag{15}$$

Here, (x_0, y_0) is the static equilibrium position of the rotor in the stationary coordinate system; F_{ind_x} and F_{ind_y} are the radial fluid forces acting on the inducer; F_{cnt_x} and F_{cnt_y} are the contact forces when the rotor contacts the casing. The parameter values of the rotor system and the simulation conditions are shown in Table 2 and Table 3.

Table 2 Parameter values of rotor system

Variables	Value	Unit
m_1	6.48	kg
k	8.023×10^7	N/m
c	456.02	N・s/m

Table 3 Condition of simulation in rotor system

Parameter	value	unit
Rotational speed ω	42500	rpm
Unbalance U	0.5×10^{-4}	kg・m

The radial fluid force acting on the inducers F_{ind_x} and F_{ind_y} is calculated from the fluid pressure

on the hub surface in the flow path. The pressure distribution $P_*(\theta_*)$ in the flow path was obtained by interpolating the three points of pressure, viz., $P_{in}, P_{m*}, and\ P_{out}$. Subsequently, the $x-$ and $y-$ direction components of the fluid force for each infinitesimal section are integrated over the entire flow path and to obtain the radial fluid force acting on the inducer. The fluid force components F_{ind_x} and F_{ind_y} were obtained by the sum of the contributions of the three flow paths.

4. Analysis of transition phenomenon from RC to AAC

4.1. Case using the nominal pump dynamics coefficients

4.1.1. Analysis procedure

The cavitation characteristics can be expressed by the pump dynamic characteristic coefficients, viz., cavitation compliance Cb and mass flow gain factor Mb, which are defined by the cavity volume V as shown in the following equation:

$$Cb = -\frac{\partial V}{\partial P_{nom}}, \quad Mb = \frac{\partial V}{\partial Q_{nom}} \tag{16}$$

Conventionally, the pump dynamic characteristic coefficients Cb and Mb are defined for all three flow paths [7][31]. These are also represented by different definitions.

$$Cb = -\frac{\partial V}{\partial \sigma_{nom}}, Mb = \frac{\partial V}{\partial \beta_{nom}} \tag{17}$$

These pump dynamic characteristic coefficients are defined as positive when cavitation grows and develops in correspondence with a decrease in the cavitation number and increase in the average value of the relative flow angle at the flow path inlet. In this study, these are referred to as nominal pump dynamic characteristic coefficients.

In this section 4.1, the nominal pump dynamic characteristics are used. A coupled analysis simulation was performed for the rotor with imbalance, and the transition from RC to AAC was investigated. The cavitation number σ was reduced, and the occurrence of the transition from RC to AAC was evaluated by investigating the changes in each flow rate and shaft vibration amplitude. The cavitation number decreased quasi-statically from 0.08 to 0.01. Based on the results of the experiments, the following two conditions are set as criteria for determining the occurrence of the transition to AAC.

(1) Only the rotation-synchronous component of the radial fluid force becomes dominant while both

the asynchronous components, i.e., the sub-synchronous and super-synchronous, disappear.

(2) Fluctuations in the flow rate of each flow path subside and become steady (because the cavity is attached to the blade).

4.1.2. Analytical result

Fig. **8** and Fig. 9 show the flow rates of each flow path when the cavitation number is 0.04 and 0.025, respectively. It can be observed in Fig. 8 that RC occurs and the flow rate fluctuates with a phase shift of 120° for each of the three flow paths. In Fig. 9 where the cavitation number was reduced from the case of Fig. 8 and the flow rate became steady, neither did the fluctuations of the flow rate of each flow path subside nor was there a transition from RC to AAC. Fig. **10** shows changes in the shaft vibration amplitude with time. Shaft vibration with an amplitude of approximately 0.1 times the clearance is generated by the fluid force owing to cavitation and the shaft imbalance. However, an increase in the shaft vibration amplitude during the transition from RC to AAC was not observed in the experiment. From the results of Fig. 8 - Fig. 10, the transition from RC to AAC was not observed and was not confirmed by performing a coupled analysis of the shaft vibration and a one-dimensional flow model of the inducer when the nominal pump dynamic characteristic coefficients were used.

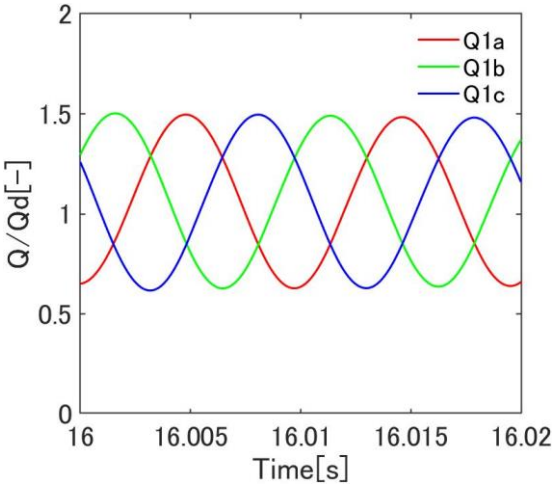

Fig. 8 Flow rate of each flow path (cavitation number 0.04)

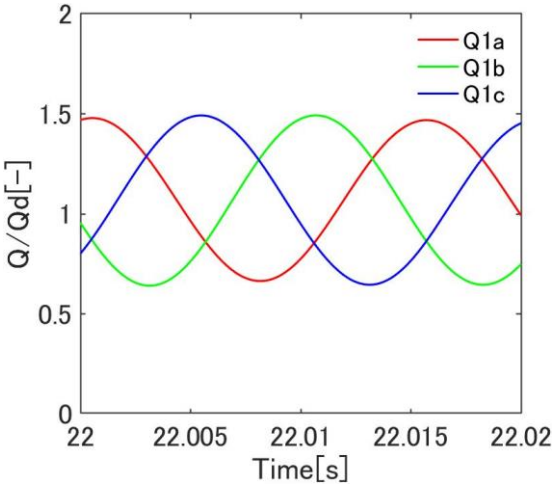

Fig. 9 Flow rate of each flow path (cavitation number 0.025)

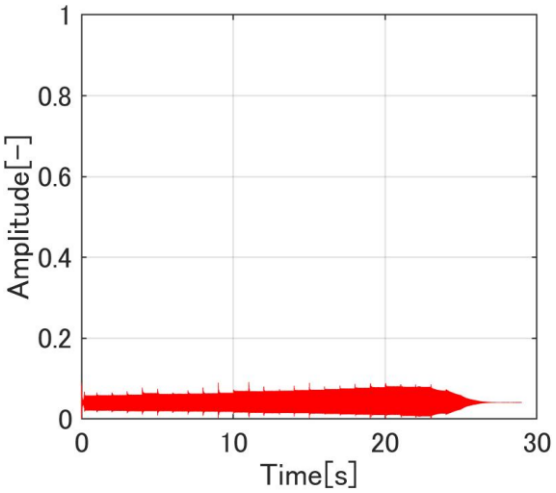

Fig. 10　Shaft vibration amplitude

4.2. Case with the pump dynamic characteristic coefficients varying with respect to the cavity length

In this section, the cavitation length is varied with respect to the cavitation number based on the experimental results of Yoshida et al. [37]. They reported that the cavity length of each flow path is different, such as "long, long, and short", when transitioning to AAC. The experimental results in Section 2 also show such changes in the lengths of the three cavities.
In this section, such changes in cavity length are considered and modeled as changes in the pump dynamics characteristic coefficients (Cb and Mb).

In the analysis, the cavitation number decreased quasi-statically over time, as shown in Fig. 15. The cavitation number is assumed to be equal in time on average in all the three flow paths (A, B, and C) up to a certain value (here, σ_{th}= 0.0275). Subsequently, the cavity length bifurcates and is set to be long in flow paths A and B and short in flow path C, when the cavitation number becomes smaller than the value σ_{th}.
Then, the occurrence of the transition from RC to AAC is examined and discussed.

In the analysis in this section, at the bifurcation of the cavity length of the flow paths, Cb and Mb of flow path C, whose cavity length is reduced, is diminished, whereas the Cb and Mb of flow paths A and B, whose cavity length is increased further, is enlarged. The reduced pump dynamic characteristic coefficients Cb and Mb of flow path C can either take a positive value, a negative value, or even 0. The situation when the pump dynamic characteristic coefficients Cb = 0 and Mb = 0 corresponds to the state in which the cavity is completely reduced.

4.2.1. Simulation using One Dimensional Flow Model of Inducer: Analysis Conditions and Results

First, a simulation of the inducer flow using a 1D flow path model was performed. The orbit of the rotor was set to a circular orbit synchronous with the shaft rotation. When the cavitation number σ is gradually reduced, the cavity length also increased corresponding with σ's change. When $\sigma = 0.0275$, the signs of the pump dynamic characteristic coefficients only in flow path C, i.e., Cb_c and Mb_c, exhibited a change. Their signs either remained unchanged, or changed from positive to negative, or became 0: six cases were investigated. Table 4 shows the pump dynamic characteristic coefficients of each flow path in each case and the case numbers are listed as 1 to 6.

Table 4 Pump dynamic characteristic coefficients pattern

	$\sigma > 0.0275$			$\sigma \leq 0.0275$			
Case number	Cb_i $(i = a,b,c)$	Mb_i $(i = a,b,c)$	Cb_i $(i = a,b)$	Mb_i $(i = a,b)$	Cb_i $(i = c)$	Mb_i $(i = c)$	Occurrence of transition ○: Occur ×:Not occur
0	Cb_{nom}	Mb_{nom}	Cb_{nom}	Mb_{nom}	Cb_{nom}	Mb_{nom}	×
1	Cb_{nom}	Mb_{nom}	Cb_{nom}	Mb_{nom}	$-Cb_{nom}$	Mb_{nom}	×
2	Cb_{nom}	Mb_{nom}	Cb_{nom}	Mb_{nom}	Cb_{nom}	$-Mb_{nom}$	×
3	Cb_{nom}	Mb_{nom}	Cb_{nom}	Mb_{nom}	$-Cb_{nom}$	$-Mb_{nom}$	○
4	Cb_{nom}	Mb_{nom}	Cb_{nom}	Mb_{nom}	0 +	Mb_{nom}	×
5	Cb_{nom}	Mb_{nom}	Cb_{nom}	Mb_{nom}	Cb_{nom}	lim to 0	×
6	Cb_{nom}	Mb_{nom}	Cb_{nom}	Mb_{nom}	lim to 0	lim to 0	×

The rightmost column of Table 4 indicates whether transition from RC to AAC occurred or not for the 6 cases: symbol ○ denotes occurrence and symbol × denotes non-occurrence. It is worth noting that transition from RC to AAC materialized only in case 3 in which both the pump dynamic characteristic coefficients, Cb_c and Mb_c, of flow path C become negative.

The simulation results for Case 3, shown in Fig. 11 and Fig. **12**, indicate the flow rates of each flow path, A, B, and C, when the cavitation number is 0.04 and 0.025, respectively. When the cavitation number is 0.04, the flow rates in paths A, B, and C fluctuate with a 120° phase shift between them, indicating the occurrence of RC. However, when the cavitation number is reduced to 0.025 the pump

dynamic characteristic coefficients of flow path C change to negative values and subsequently the fluctuations in the flow rate of flow paths A, B, and C settle down and the flow becomes steady.

The transition from RC to AAC which was observed in the experiment is reaffirmed here by considering the change in the sign of the pump dynamic characteristic coefficients. In the next section, the experimental results shown in Fig. 4 are verified by a coupled analysis of the rotor vibration and 1D flow in the flow paths of the inducer.

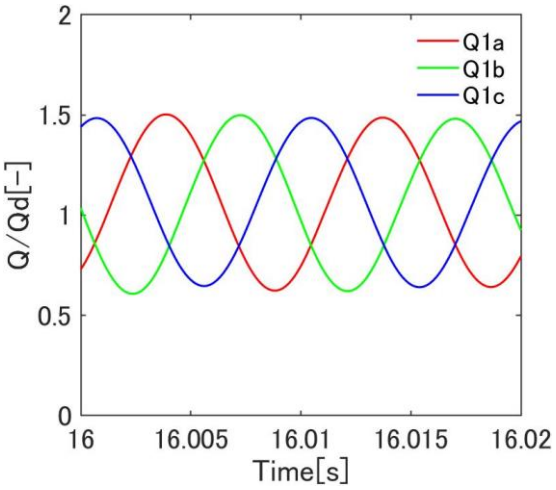

Fig. 11 Flow rate of each flow path (cavitation number 0.04)

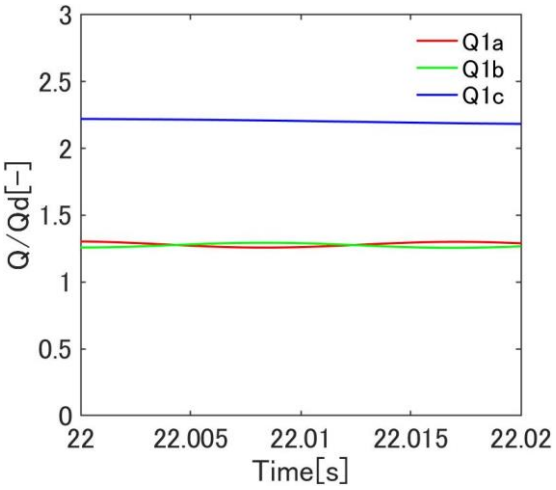

Fig. 12 Flow rate of each flow path (cavitation number 0.025)

4.2.2. Validity examination of negative pump dynamic characteristic coefficient

In the previous section, the sign of the pump dynamic characteristic coefficient of flow path C was set to negative, based on intuitive considerations. In this section, the validity of the sign of the pump dynamic characteristic coefficient is negative.

The cavity lengths bifurcate when the cavitation number decreases. The changes in the cavity length and width of each flow path, assuming that A and B are the flow paths whose cavity lengths are lengthened and C is the flow path whose cavity length is shortened, are shown in Fig. 13 and Fig. **14** [41].

RC occurs in the region before the bifurcation of the cavitation size (blue region in Fig. 13 and Fig.

14 the average values of the cavity length and width for the three flow paths do not change with time. Therefore, the nominal values of the cavity length and width, l_{nom} and w_{nom}, and the corresponding pump dynamic characteristic coefficients, Cb_{nom} and Mb_{nom}, are used for each flow path. Further, it should be noted that $\partial l_{nom}/\partial\sigma_{nom} < 0$, $\partial w_{nom}/\partial\sigma_{nom} < 0$.

In the region after bifurcation (red region in Fig. 13 and Fig. **14**), the cavity length and width of each flow path are represented by l_i and w_i and the corresponding pump dynamic characteristic coefficients are represented by Cb_i and Mb_i, respectively: the symbols $i = a, b, c$ represent each flow path number. From the experimental results of Yoshida [37] and Huang et al. [41] it is known that $\partial l_{a,b}/\partial\sigma_{nom} < 0, and\ \partial w_{a,b}/\partial\sigma_{nom} < 0$ for flow paths A and B, whereas $\partial l_c/\partial\sigma_{nom} > 0, and\ \partial w_c/\partial\sigma_{nom} > 0$ for flow path C.

Based on the above conditions, the relationships between the pump dynamic characteristics before and after bifurcation of the cavity length and width were investigated.

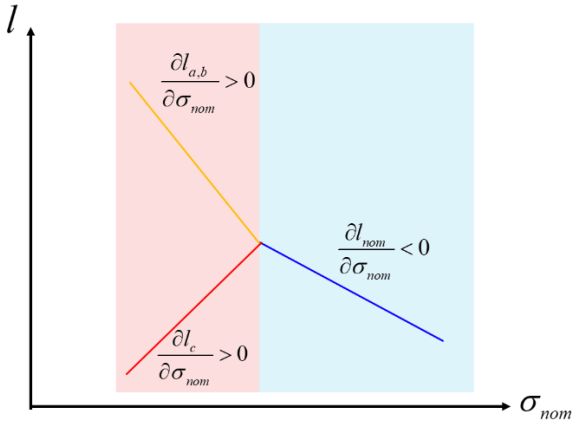

Fig. 13 Variation of cavity length of three-bladed inducer

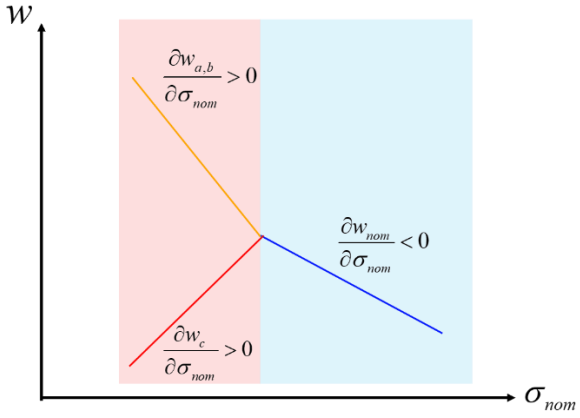

Fig. 14 Variation of cavity width of three-bladed inducer

(a) Cavitation compliance Cb

First, the cavitation compliance, Cb is considered. The nominal value Cb_{nom} is expressed in Eq. (17) using the following equation with the nominal cavity volume V_{nom}.

$$Cb_{nom} \equiv -\frac{\partial V_{nom}}{\partial \sigma_{nom}} \tag{18}$$

Here, the nominal cavity volume V_{nom} is expressed by the following equation using the nominal cavity length l_{nom}, nominal cavity width w_{nom}, and nominal cavity height h.

$$V_{nom} = l_{nom} w_{nom} h \tag{19}$$

From equations (18) and (19) and assuming that h is constant during the change in σ_{nom}, the following equation holds:

$$Cb_{nom} \equiv -\frac{\partial V_{nom}}{\partial \sigma_{nom}} = -\frac{\partial (l_{nom} w_{nom} h)}{\partial \sigma_{nom}} = -h\left(w_{nom} \frac{\partial l_{nom}}{\partial \sigma_{nom}} + l_{nom} \frac{\partial w_{nom}}{\partial \sigma_{nom}} \right) \tag{20}$$

Considering the relationship between Cb_c of flow path C after the bifurcation and the nominal value Cb_{nom}, the following expression holds:

$$V_c = l_c w_c h,$$
$$Cb_c \equiv -\frac{\partial V_c}{\partial \sigma_{nom}} = \frac{w_c \frac{\partial l_c}{\partial \sigma_{nom}} + l_c \frac{\partial w_c}{\partial \sigma_{nom}}}{w_{nom} \frac{\partial l_{nom}}{\partial \sigma_{nom}} + l_{nom} \frac{\partial w_{nom}}{\partial \sigma_{nom}}} Cb_{nom} \tag{21}$$

From the assumptions in Figs. 14 and 15, $\partial l_{nom}/\partial \sigma_{nom} < 0$, $\partial w_{nom}/\partial \sigma_{nom} < 0$, and Cb_{nom} is positive before the bifurcation. Conversely, $\partial l_c/\partial \sigma_{nom} > 0$ and $\partial w_c/\partial \sigma_{nom} > 0$ in flow path C after bifurcation and Cb_c in flow path C can be negative.

(B) Mass flow gain factor Mb

Next, the mass flow gain factor, Mb is considered. The nominal value Mb_{nom} expressed in Eq. (17) can also be expressed in the following form while applying the average cavity volume V_{nom}.

$$Mb_{nom} \equiv \frac{\partial V_{nom}}{\partial \bar{\beta}_{nom}} = \frac{\partial (l_{nom} w_{nom} h)}{\partial \bar{\beta}_{nom}} = h\left(w_{nom} \frac{\partial l_{nom}}{\partial \bar{\beta}_{nom}} + l_{nom} \frac{\partial w_{nom}}{\partial \bar{\beta}_{nom}} \right) \tag{22}$$

Here, $\bar{\beta}_{nom}$ is the average value of the relative flow angle at the flow path inlet. This is a uniquely determined value for all flow paths, similar to the cavitation number σ_{nom}. Because the fluid has the property of flowing along the surface of cavitation [33], as the cavitation number σ_{nom} decreases both the cavitation width as well as the cavity length increase. Subsequently, the flow velocity in the axial direction decreases owing to the increase in cavity volume, and the average value of the relative flow angle at the flow path inlet $\bar{\beta}_{nom}$ increases. Thus, σ_{nom} and $\bar{\beta}_{nom}$ satisfy the following relational expressions:

$$\frac{\partial \bar{\beta}_{nom}}{\partial \sigma_{nom}} < 0 \tag{23}$$

Because the cavity length does not contribute to the average value of the relative flow angle at the flow path inlet, let $\partial l_c / \partial \bar{\beta}_{nom} = \partial l_{nom} / \partial \bar{\beta}_{nom} = 0$, the relationship between Mb_{nom} before the bifurcation and Mb_c in flow path C after the bifurcation is represented as follows:

$$\begin{aligned} Mb_c &\equiv \frac{\partial V_c}{\partial \bar{\beta}_{nom}} \\ &= \frac{\dfrac{\partial (w_c l_c)}{\partial \bar{\beta}_{nom}}}{\dfrac{\partial (w_{nom} l_{nom})}{\partial \bar{\beta}_{nom}}} Mb_{nom} = \frac{\dfrac{\partial (w_c l_c)}{\partial \sigma_{nom}} \dfrac{\partial \sigma_{nom}}{\partial \bar{\beta}_{nom}}}{\dfrac{\partial (w_{nom} l_{nom})}{\partial \sigma_{nom}} \dfrac{\partial \sigma_{nom}}{\partial \bar{\beta}_{nom}}} Mb_{nom} = \frac{\dfrac{\partial (w_c l_c)}{\partial \sigma_{nom}}}{\dfrac{\partial (w_{nom} l_{nom})}{\partial \sigma_{nom}}} Mb_{nom} \end{aligned} \tag{24}$$

Here, $Mb_c < 0$ is obtained from $\partial (l_c w_c) / \partial \sigma_{nom} > 0$ and $\partial (l_{nom} w_{nom}) / \partial \sigma_{nom} < 0$ after the bifurcation.

From the above, it was confirmed that the pump dynamic characteristic coefficients Cb_c and Mb_c of flow path C, whose cavity length is shortened after bifurcation, can both have negative signs.

5. Coupled analysis of shaft vibration and fluid flow in inducer

In the previous section, the fluid flow analysis of the inducer using the 1D flow path model was performed. Subsequently, the transition from RC to AAC in the flow rates of all three flow paths was observed by introducing the change of sign in the pump dynamic characteristics corresponding to the change in cavity length for each flow path.

In this section, a coupled analysis of the 1D flow path and shaft vibration models by incorporating changes in the pump dynamic characteristic coefficient corresponding to the change in the cavity length is presented. Shaft imbalance was applied to the shaft vibration model, and the numerical simulation of the coupled system was performed by decreasing the cavitation number, as in the experiment. Additionally, changes in shaft vibration behavior during the transition from RC to AAC was investigated.

5.1. Analysis condition

As shown in Fig. 15, the cavitation number decreases quasi-statically. It is assumed that bifurcation occurs in the cavity length, as in Section 4.2.2 (Fig. 13), when the cavitation number reaches σ = 0.0275. The cavity length of flow path C becomes shorter and the signs of the pump dynamic characteristic coefficients, i.e., Cb_c and Mb_c, become negative. Changes in the pump dynamic characteristic coefficient are the same as that shown for Case 03 in Table 4. The parameter values are the same as those shown in Table 3 in Section 3.3.

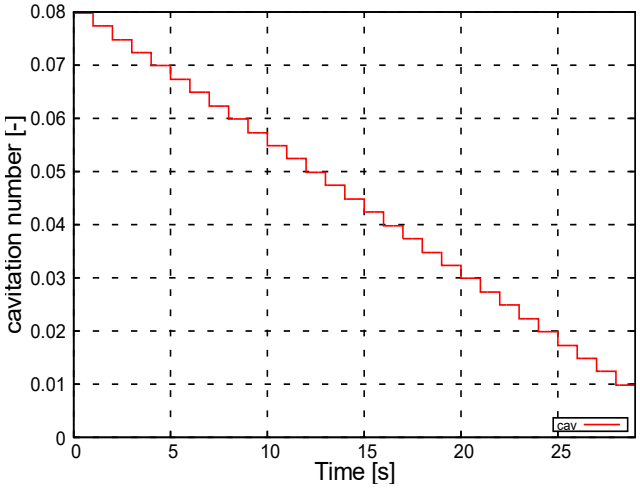

Fig. 15 Given time history of cavitation number

5.2. Analysis results

Fig. 16 and Fig. 17 show the flow rates of each flow path obtained in the coupled analysis of the shaft vibration system and the 1D flow path model when the cavitation number is 0.04 and 0.025, respectively. Fig. 16 shows that the flow rate fluctuation of the RC appears when the cavitation number is σ = 0.04. Subsequently, the flow becomes steady in Fig. 17 where the cavitation number σ = 0.025, which is lower than that at bifurcation (σ = 0.0275). These figures indicate the occurrence of transition from RC to AAC.

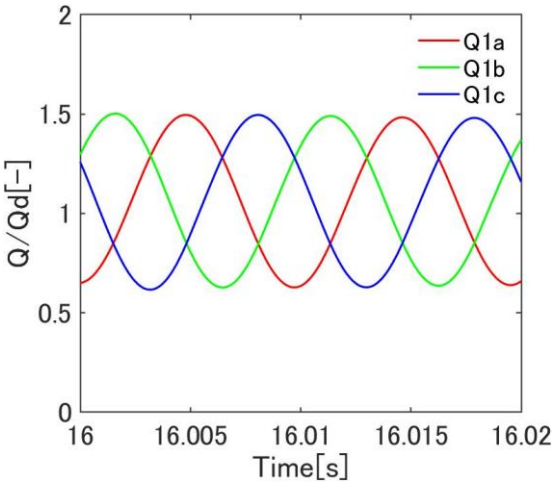

Fig. 16 Flow rate of each flow path (cavitation number 0.04)

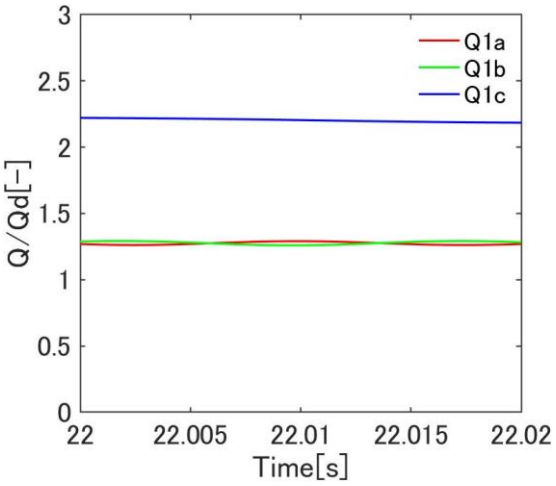

Fig. 17 Flow rate of each flow path (cavitation number 0.025)

Fig. 18 shows the changes in shaft vibration amplitude with time, and Fig. 19 shows the frequency-

amplitude change in shaft vibration obtained from the coupled analysis. Both figures Fig. 18 and Fig. **19** that the shaft vibration amplitude increases sharply when the cavitation number reaches the value at which bifurcation occurs (σ = 0.0275). Moreover, Fig. 19 shows that the super-synchronous vibration component of the RC is entrained to the synchronous component at bifurcation point and the synchronous component increases sharply and becomes dominant.

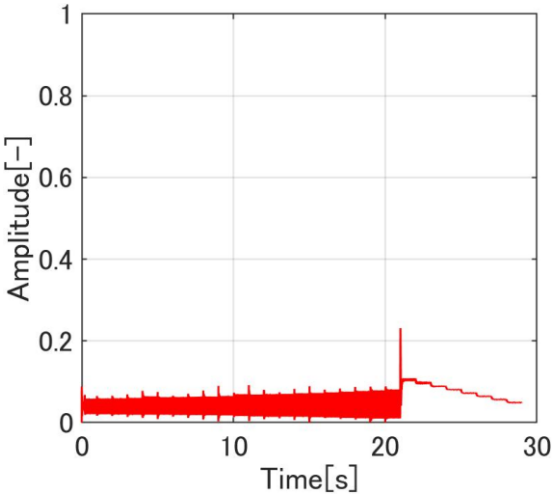

Fig. 18 Shaft vibration amplitude

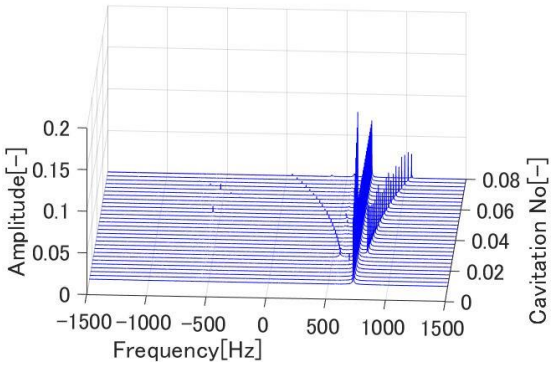

Fig. 19 Waterfall diagram of shaft vibration amplitude

In the experiment shown in Fig. 4, it was observed that the shaft vibration amplitude of the synchronous component at the transition to AAC was approximately 1.5 times higher than that at RC. Similarly, the increase in the shaft vibration amplitude of the synchronous component in this coupled analysis also shows a significant change in the order of the same degree.

Fig. **20** shows the change in pressure coefficient C_p, and it can be observed that the pressure coefficient decreased when the cavitation number reached one at bifurcation (σ = 0.0275), which is consistent with the experimental results. During the time period with AAC, in the flow path where the cavity length is enlarged to some extent with respect to the blade length, the pressure coefficient decreases owing to blockage of this flow path caused by increase in the cavity volume. Fig. 20 indicates that this phenomenon was reproduced in this coupled analysis.

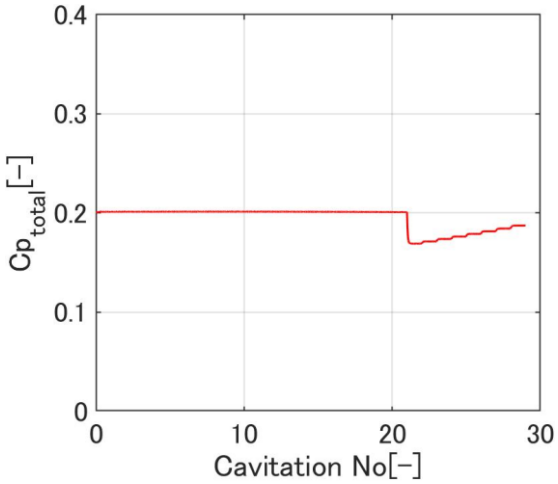

Fig. 20 Pressure coefficient (cavitation number 0.025)

6. Conclusion

A coupled analysis of a one-dimensional flow path flow model of 3-blade inducer and shaft vibration system was conducted, and the transition from RC to AAC was investigated. The following conclusions were drawn:

From the results of the water tunnel tests conducted in this study and the experimental results in the literature, it is evident that the cavity length rapidly changed at the occurrence of AAC. The individual cavity length changed with respect to the cavitation number. This phenomenon was modeled by changes in the pump dynamic characteristic coefficients.

The facts that the cavity length bifurcates and the cavity length changes individually is incorporated as a change in the sign of the pump dynamic characteristic coefficients. A numerical analysis using a 1D flow path flow model revealed that the transition from RC to AAC occurs only when the signs of the pump dynamic characteristic coefficients (both cavitation compliance and mass flow gain factor) become negative.

A coupled analysis of the 1D flow path flow model and shaft vibration was performed by considering the effect of bifurcation of the cavity length on the pump dynamic characteristic coefficients. The signs

of the pump dynamic characteristic coefficients (both cavitation compliance and mass flow gain factor) were set as negative at the bifurcation. The results of the coupled analysis were qualitatively in good agreement with the experimental results obtained from the water tunnel test.

Acknowledgement

The authors thank Mr. Hayate Okawa for his assistance with the analytical and experimental results.

References

[1] A. Okayasu, T. Ohta, T. Azuma and H. Aoki. “Vibration Problem in the LE-7 Liquid Hydrogen Turbopump.” Proc. AIAA/SAE/ASME/ASEE 26th Joint Propulsion Conference, AIAA 90-2250 (1990). doi:10.2514/6.1990-2250

[2] de Bernardi J., Joussellin F. and Von Kaenel A. Experimental Analysis of Instabilities Related to Cavitation in Turbopump Inducer. 1st Int. Symp. on Pump Noise and Vibrations, pp. 91-99. Paris, France (1993)

[3] Yoshinobu Tsujimoto, Kenjiro Kamijo, Christopher Brennen, “Unified Treatment of Flow Instabilities of Turbomachines”, Journal of Propulsion and Power Vol.17, No.3, May-June 2001, doi:10.2514/2.5790

[4] Masaharu Uchiumi, Kenjiro Kamijo, Kunio Hirata, Akira Konno, Tomoyuki Hashimoto and Satoshi Kobayashi, “Improvement of Inlet Flow Characteristics of LE-7A Liquid Hydrogen Pump”, Journal of Propulsion and Power Vol.19, No.3, May-June 2003. doi:10.2514/2.6139

[5] Kenjiro Kamijo, Takashi Shimura. and Mitsuo Watanabe., “An Experimental Investigation of Cavitating Inducer Instability”, ASME paper, 77-WA/FE-14 (1977)

[6] Pagnier P, Morel P., Spettel F., Henry C &Champagne J-Y. Conception and experimental study of an inducer. In Cav'95 Int. Symp., Deauville, France (1995).

[7] Takashi Shimura, ”Geometry Effects in the Dynamic Response of Cavitating LE-7 Liquid Oxygen Pump” Journal of Propulsion and Power, Vol.11 (1995): 330–336.

[8] Yoshinobu Tsujimoto, Kenjiro Kamijo. and Yoshiki Yoshida, “A Theoretical Analysis of RC in Inducers”, Trans. ASME, Journal of Fluids Engineering, Vol. 115 (1993): 135–141. doi:10.1115/1.2910095

[9] Joussellin F. & De Bernardi J. (1994). Analytical Modelling of Instabilities in a Cavitating

Turbopump Inducer. In 2nd Int. Symp. on Cavitation, pp. 98-94, Tokyo, Japan.

[10] Pilipenko V., Semyonov Y. & Kvasha Y. Theoretical and Experimental Computational Methods for Determining Volume of Cavities and Coefficients of Dynamic Equation of Cavitation Cavities. Tech. Rep.. SEP TC/T 23227/96 (1995).

[11] Satoshi Watanabe, Kotaro Sato, Yoshinobu Tsujimoto, Kenjiro Kamijo, "Analysis of RC in a Finite Pitch Cascade Using a Closed Cavity Model and a Singularity Method", Journal of Fluids Engineering, 121(4), 834–840 (Dec 01, 1999) (7 pages), doi:10.1115/1.2823544

[12] Reboud J-L. & Delannoy Y. Two-phase flow modelling of unsteady cavitation. 2nd Int. Symp. on Cavitation, Tokyo (1994)

[13] Delannoy, Y. & Kueny, J.L. Two phase flow approach in unsteady cavitation modelling. Cavitation and Multiphase Flow Forum, ASME-FED vol.98, pp. 153-158. (1990)

[14] Coutier-Delgosha O., Reboud J-L.& Albano G.. Numerical Simulation of the Unsteady Cavitating Behaviour of an Inducer Blade Cascade. Proc. ASME Fluids Engineering Summer Conference. Boston Massachusetts. (2000)

[15] F. Joussellin, Y. Courtot, O. Coutier-Delgosha, J.L. Reboud, Cavitating Inducer Instabilities: Experimental Analysis And 2d Numerical Simulation Of Unsteady Flow In Blade Cascade, 4th Int. Symposium on Cavitation, sessionB8.002, Pasadena (USA) 2001

[16] O. Coutier-Delgosha, J. Perrin, R Fortes Patella and J.L. Reboud, A Numerical Model To Predict Unsteady Cavitating Flow Behaviour In Inducer Blade Cascades, Fifth International Symposium on Cavitation (CAV2003),CAV03-OS-4-005, Osaka,Japan, Nov.1-4, 2003

[17] Olivier Coutier-Delgosha, Yannick Courtot, Florence Joussellin, and Jean-Luc Reboud, Numerical Simulation of the Unsteady Cavitation Behavior of an Inducer Blade Cascade, AIAA JOURNAL, Vol. 42, No. 3, March 2004, pp560-569.

[18] Angelo Cervone, Renzo Testa, Cristina Bramanti, Emilio Rapposelli and Luca d'Agostino, Thermal Effects on Cavitation Instabilities in Helical Inducers, Journal of Propulsion and Power 21(5),pp.893-899, September 2005

[19] Giovanni Pace, Dario Valentini, Angelo Pasini, Lucio Torre, Yanxia Fu and Luca d'Agostino, Geometry Effects on Flow Instabilities of Different Three-Bladed Inducers, Trans of ASME, J. Fluids Eng. Apr 2015, 137(4): 041304 (12 pages) https://doi.org/10.1115/1.4029113

[20] Y. Wan, M. Manfredi, A. Pasini, Z. Spakovszky, Dynamic Model-Based Identification of Cavitation Compliance and Mass Flow Gain Factor in Rocket Engine Turbopump Inducers , Trans of ASME, J. Eng. Gas Turbines Power., 2021, 143(2): 021011 (10 pages), https://doi.org/10.1115/1.4049015

[21] Luca Sales, Angelo Pasini, Definition and Validation of Cavitating Rocket Turbopump

Transmission Matrices for Modular Multi Actuator Disk Approach, Trans of ASME, J. Fluids Eng.,2021, 143(12): 121110 (9 pages), https://doi.org/10.1115/1.4052045

[22] Angelo Pasini, Ruzbeh Hadavandi, Dario Valentini, Giovanni Pace, Luca d'Agostino, Dynamics of the Blade Channel of an Inducer Under Cavitation-Induced Instabilities, Trans of ASME, J. Fluids Eng., 2019, 141(4): 041103 (11 pages), https://doi.org/10.1115/1.4041728

[23] Giovanni Pace, Dario Valentini, Angelo Pasini, Ruzbeh Hadavandi, Luca d'Agostino, Analysis of Flow Instabilities on a Three-Bladed Axial Inducer in Fixed and Rotating Frames, Trans of ASME, J. Fluids Eng. Apr 2019, 141(4): 041104 (13 pages), https://doi.org/10.1115/1.4041731

[24] Dario Valentini, Giovanni Pace, Lucio Torre, Angelo Pasini, Luca d'Agostino, Influences of the Operating Conditions on the Rotordynamic Forces Acting on a Three-Bladed Inducer Under Forced Whirl Motion, Trans of ASME, J. Fluids Eng. Jul 2015, 137(7): 071304 (10 pages), https://doi.org/10.1115/1.4029887

[25] Yuka Iga, Motohiko Nohmi, Akira Goto and Toshiaki Ikohagi. "Numerical Analysis of Cavitation Instabilities Arising in the Three-Blade Cascade", Trans. ASME, Journal of Fluids Engineering, Vol. 126 (2004), pp. 419–429. doi: 10.1115/1.1760539

[26] Hosangadi, A., Ahuja, V., and Ungenwitter, R., Simulations of Rotating Cavitation Instabilities in the SSME LPFP Inducer, 43rd AIAA/ASME/SAE/ASEE Joint Propulsion Conference and Exhibit, AIAA Paper 2007-5536, July 2007.

[27] Benoît Pouffary, Regiane Fortes Patella, Jean-Luc Reboud and Pierre-Alain Lambert, Numerical analysis of cavitation instabilities in inducer blade cascade, Trans of ASME, J. Fluids Eng. Apr 2008, 130(4): 041302 (8 pages) https://doi.org/10.1115/1.2903823

[28] R. Fortes-Patella, O. Coutier-Delgosha, J. Perrin and J. L. Reboud, Numerical Model to Predict Unsteady Cavitating Flow Behavior in Inducer Blade Cascades, Trans of ASME, J. Fluids Eng. Feb 2007, 129(2): 128-135 (8 pages) https://doi.org/10.1115/1.2409320

[29] An Byungjin, and Takeo Kajishima, "Transition from RC to Cavitation Surge in a Two-Dimensional Cascade", Journal of Fluid Science and Technology, Vol.8, No.1, 2013:20–29. doi:10.1299/jfst.8.20

[30] Chang-Ho Choi and Jinhan Kim, Study on the Cavitating Flows in a Turbopump Inducer, JOURNAL OF PROPULSION AND POWER, Vol. 31, No. 2, March–April, 2015, https://doi.org/10.2514/1.B35216

[31] Takashi Shimura, Satoshi Kawasaki and Masaharu Uchiumi, "One-dimensional Multidomain Analysis of RC", Transactions of the JSME, Vol. 815, No. 829 (2015) doi: 10.1299/transjsme.15-00125, In Japanese

[32] Satoshi Kawasaki, Takashi Shimura, Masaharu Uchiumi and Yuka Iga, "One-Dimensional

Analysis Method for Cavitation Instabilities of a Rotating Machinery", Trans. ASME, Journal of Fluids Engineering, Vol. 140(2) (2018). doi: 10.1115/1.4037987

[33] Hironori Horiguchi, Satoshi Watanabe, Yoshinobu Tsujimoto and Masanori Aoki, "A Theoretical Analysis of Alternate Blade Cavitation in Inducers", Trans. ASME, Journal of Fluids Engineering, Vol. 120(1) (2000), pp. 156–163. doi: 10.1115/1.483238

[34] Hironori Horiguchi,"Steady Flow and Stability Analyses of Cavitation in Finite Blade Count Impeller" Trans. JSME, Vol.65, No.636 (1999) In Japanese

[35] R Campos-Amezcua, S Kehelladi, F Bakir, Z Mazur-Czerwiec,C Sarraf, and R Rey, Numerical analysis of unsteady cavitating flow in an axial inducer, Proc. IMechE Vol. 224 Issue 2 Part A: J. Power and Energy, 2010, pp.223-238, DOI: 10.1243/09576509JPE647

[36] Satoshi Kobayashi, "Effects of Shaft Vibration on the Occurrence of the Asymmetric Cavitation in an Inducer", JSME International Journal Series B, Vol.49, No.4 (2006), pp. 1220–1225. doi: 10.1299/jsmeb.49.1220

[37] Yoshiki Yoshida, "Rotordynamic Forces Acting on Three-Bladed Inducer Under Supersynchronous/Synchronous RC" Trans. ASME, Journal of Fluids Engineering, Vol. 132(6) (2010), 061105. doi: 10.1115/1.3425727

[38] Ruzbeh Hadavandi, Giovanni Pace, Dario Valentini, Angelo Pasini and Luca d'Agostino, Identification of Cavitation Instabilities on a Three-Bladed Inducer by Means of Strain Gages, Trans of ASME, J. Fluids Eng. Feb 2020, 142(2): 021210 (10 pages) https://doi.org/10.1115/1.4045186

[39] Moena Kanamaru, Yoshito Kamikura, Satoshi Kawasaki, Takashi Shimura,and Iga Yuka, An experimental study of influence of slits in throat position on supression of cavitation instabilities in liquid propellant rocket inducer, AJK 2019 Joint Fluid Engineering Conference, 2019-4838, 2019(7 pages) San Franisco, USA

[40] Bjorn Gwiasda, Matthias Mohr, Martin Bohle, "Investigations of Inducers Operating with High Rotational Speed", International Symposium on Transport Phenomena and Dynamics of Rotating Machinery(ISROMAC 2017), Maui Hawaii, 2017

[41] Jian-De Huang, Masanori Aoki and Jian-Tong Zhang, "Alternate Blade Cavitation on Inducer", JSME International Journal Series B Fluids and Thermal Engineering 41, no. 1 (1998): 1–6.

[42] Claudio Lettieri, Zoltan Spakovszky, David Jackson and Vincent Wang, Characterization of Rotating Cavitation in a Four Bladed Inducer, 52nd AIAA/SAE/ASEE Joint Propulsion Conference 2016-4986, 2016, https://doi.org/10.2514/6.2016-4986

[43] C. Lettieri, Z. Spakovszky, D. Jackson and J. Schwille, Characterization of Cavitation Instabilities in a Four-Bladed Turbopump Inducer,AIAA JOURNAL OF PROPULSION AND POWER, Vol. 34, No. 2, 2017, pp.510-520, https://doi.org/10.2514/1.B36317

[44] A. G. Vermes, C. Lettieri, Source Term Based Modeling of Rotating Cavitation in Turbopumps, Trans. of ASME, J. Eng. Gas Turbines Power. 2019, 141(6): 061002 (8 pages), https://doi.org/10.1115/1.4042302